Section: Research Paper

OPHTHALMOLOGY GLAUCOMA DETECTION USING VGG 16 CNN-MODIFIED DENSENET ARCHITECTURE IN RETINAL FUNDUS IMAGES

Dr R. Deepa Associate Professor[1] Orchid 0000-0001-7010-2983
rdeepa1981@gmail.com
[1]Department of Computer Science, PSG College of Arts & Science
Coimbatore 641014, Tamilnadu.

S.Vaishnavi Research Scholar[2] Orchid 0000-0003-1170-0662
vaish18kumar@gmail.com
[2]Department of Computer Science, PSG College of Arts & Science
Coimbatore 641014, Tamilnadu.

Abstract
Glaucoma is a serious eye disease that can cause irreversible vision loss, making early diagnosis and treatment essential. In this study, we propose a novel hybrid deep learning-based method for identifying glaucoma in retinal images. Our approach involves training a hybrid neural network using a modified VGG16 architecture based on a CNN-modified DenseNet architecture, optimizing with an improved Adam optimization algorithm, and applying image denoising with both adaptive and non-adaptive thresholding. To smooth out the retinal images, we use anisotropic diffusion filtering instead of the conventional median filter method. For segmentation of retinal images, we employ a cascading UNet architecture, where each iteration of segmentation builds upon the results of the previous iteration, leading to more precise glaucoma diagnosis, even at the early stages of the disease. To evaluate the performance of our suggested technique, we conducted extensive trials using a publicly available collection of retinal images. Our results indicate that our proposed approach outperforms the state-of-the-art in glaucoma detection, achieving higher accuracy, sensitivity, and specificity. Our approach has the potential to significantly improve early glaucoma detection and treatment, thereby reducing the risk of blindness.

Keywords: Glaucoma, Image Denoising, Cascaded Unet Segmentation, Hybrid Neural Network

I. INTRODUCTION

Millions of people are affected by glaucoma, making it the leading cause of blindness globally [1]. Early detection and treatment of glaucoma are critical for preventing permanent vision loss [2]. CAD systems that analyze retinal images have shown promise in expediting the detection of glaucoma at an earlier stage [3]. Yet, due to the complexity of retinal images and the subtle disease-related modifications, accurate diagnosis of glaucoma remains challenging [4].

Glaucoma is a progressive and complex eye disease that affects the optic nerve, which sends visual information from the eye to the brain. It is the leading cause of blindness worldwide, particularly among people over the age of 60 [5]. Glaucoma symptoms may not appear until the illness has caused significant damage. Glaucoma risk factors include age, family history,

excessive ocular pressure, and certain medical illnesses such as diabetes and hypertension [6]. While there is no cure for glaucoma, early detection and treatment may help to postpone or prevent vision loss [7]. Early detection of glaucoma necessitates frequent eye exams, particularly for those at high risk.

As a solution, we provide a novel deep learning-based technique for glaucoma detection that combines picture denoising with cascaded UNET segmentation [8]. The suggested method is comprised of many parts, such as the following: dataset training using a hybrid neural network VGG16 with a CNN-modified Densnet architecture; optimisation with an improved Adam optimisation algorithm; and image denoising with adaptive and non-adaptive thresholding [9]. Together with this, we utilise anisotropic diffusion filtering, which is similar to the standard median filter method, to remove unwanted noise from retinal images [10].

By using a cascading UNET architecture, we successfully segment pictures for glaucoma detection. Several iterations of UNET segmentation are used in this architecture, with results from each iteration building on those of the previous iteration [11]. This paves the way for a precise glaucoma diagnosis in the retinal images, even at the early stages of the disease [12].

We conducted extensive trials using a publicly available collection of retinal images to test the performance of our suggested technique [13-17]. We found evidence that the suggested technique for detecting glaucoma is more accurate, sensitive, and specific than the state-of-the-art approaches now in use [18-21].

The danger of blindness may be greatly reduced with the use of the technology we propose. In this work, we first provide a novel method for glaucoma diagnosis that makes use of state-of-the-art deep learning techniques, and then we use extensive trials and comparisons to existing approaches to prove that our suggested method is superior.

II. BACKGROUND STUDY

Atheesan S., & Yashothara S. [1] “When compared to the current method of diagnosing glaucoma with naked human eyes, which was time consuming, labour intensive, and requires a higher level of expertise from the personnel involved, "Automated Glaucoma Detection" provides a more satisfactory solution to the issues and shortcomings that have been raised. A doctor's diagnosis of this kind of eye disease was also suspect. Some study has been done in the past, but most things in Sri Lanka were still done manually. Many people in underdeveloped areas become blind because there aren't enough eye doctors to care for them. One possible solution to these issues was to implement an automated diagnostic system. The proposed method can detect glaucoma since it involves the calculation of CDR.

Jain, S., & Salau, A. O. [5] If glaucoma, an illness of the optic nerve, isn't treated quickly, it might lead to permanent blindness. Early glaucoma detection was currently a major focus of medical research. Many methods have been developed over the years to help diagnose glaucoma, however they tend to be expensive and have low detection accuracies. The main purpose of this research was to use 2D Tensor EWT to distinguish between healthy and glaucomatous eye images. The EWT components and frequency spectra of all 2D channels were analysed. The t test method was used after computing Correntropy characteristics to choose the most advantageous ones. Ten cross validation techniques were utilised to determine the optimum characteristics for the SVM classifier to employ when classifying normal and glaucoma images.

Karmawat, R. [7] The proposed method presents a fusion feature classification and optic cup segmentation based automated glaucoma detection mechanism. An in-painting method for removing vascular anatomy was developed using a combination of median filtering and inward

interpolation approaches. The optic cup was divided using FCM clustering, and then its rough edges were smoothed down using an elliptical curve fitting technique.

Kumar, B. [9] In this research, the author analysed the many methods used to detect glaucoma. Glaucoma was a major contributor to preventable blindness across the world. The author need to develop a less expensive automated approach for diagnosing glaucoma illness so that the author can rely on the present diagnostic tools. There may be a need for these methods in places where ophthalmologists were few, such as in poor countries. Possible future benefits for the poor might come from more accurate detection at lower costs. There was hope for preventing total blindness from glaucoma if the disease was detected and treated early.

Panda, R. [13] To help ophthalmologists with widespread glaucoma screening, the author provide a new technique for identifying RNFLD. Training the RNN with newly generated patch characteristics allows for the identification of the authentic border pixels. The proposed method was evaluated, and it was shown to be effective in detecting RNFLDs on the freshly produced dataset with a high degree of accuracy.

Raja, H. [15] In this research paper, the author provide a method for analysing a B-scan OCT image for the detection of glaucomatous optic nerve damage. It was previously believed that the cup-to-disc ratio was a good indicator of glaucoma. The CDR was computed after the RPE and ILM layers have been eliminated. To train the model, the author just use a single convolutional neural network (CNN) using data from healthy and glaucoma eyes. The suggested procedure is quite similar to that used by a manual ophthalmologist to remove the inner limiting membrane and retinal pigmented epithelium. The suggested solutions' durability was a result of their reduced reliance on picture quality and other artefacts' impacts. We found that the novel method significantly outperformed the existing state-of-the-art methods.

Sarkar, D., & Das, S. [17] The CDR was a measure of how many people have glaucoma as an indication. The effectiveness of picture files stored in the RIM-ONE database may be gauged using the method the author propose. In contrast to high precision, high recall summarises the most important discoveries. A better result was achieved by increasing specificity, sensitivity, and accuracy.

III. MATERIALS AND METHODS

3.1 Dataset

This dataset can be used for training and testing machine learning models for Glaucoma Detection, including image classification, segmentation, and other tasks. However, it should be noted that the dataset is relatively small and may not be sufficient for training complex models. **https://www.kaggle.com/datasets/sshikamaru/glaucoma-detection** Each image in the dataset is labeled as either "Glaucoma" or "Normal" by an expert ophthalmologist. The dataset is balanced, with 1,413 images labeled as "Glaucoma" and 1,413 images labeled as "Normal".

3.2 Image dataset training using Hybrid Neural network

The image dataset training process for Glaucoma Detection using a Hybrid Neural Network of VGG16 with CNN-modified Densenet involves multiple steps. First, a dataset of images related to glaucoma and healthy eyes is collected and pre-processed. The images are resized and normalized to ensure consistency in image size and quality. This pre-processing step is crucial for achieving optimal performance of the neural network.

Next, the VGG16 architecture is utilized as the backbone of the neural network. This architecture is known for its deep convolutional layers that can effectively learn high-level features from input images. The pre-trained VGG16 model is then fine-tuned on the specific glaucoma dataset to enhance its ability to detect features related to glaucoma. To further improve

the performance of the neural network, a CNN-modified Densenet is integrated into the VGG16 model. This modification allows for the extraction of features at different scales and resolutions, which can improve the overall accuracy of the model. The Densenet architecture also helps to reduce the number of parameters in the network and prevent overfitting.

The HNN model is based on a three-layer architecture similar to that of conventional ANNs, but with the addition of novel activation functions. Using the fuzzy pattern-recognition approach, we may build a conceptual function from the input layer to the hidden layer, as shown below.

$$q_i = \frac{1}{\sum_{j=1}^{k}\left[W_{ij}\left(q_j^{im} - m_i\right)\right]^2} \text{ ---- (1)}$$

3.1 CNN with Improved Densenet

Networks of convolutional neural networks (CNNs) are a kind of deep learning system that can take an image as input and distinguish between identical pictures by assigning weights to various features of the image. As compared to other classification methods, CNN needs much less preprocessing. CNN may learn to produce filters after being exposed to training data, while this was previously a human process.

In theory, CNNs are analogous to the human brain, with each neuron only responding to stimuli that fall inside its receptive field. Several of these receptors work together to comprehend what we see as humans. To a large extent, the effectiveness of Convolutional Neural Networks is dependent on their initial settings.

• Input Image
• CNN
• Output Label (Image Class)

By capitalising on the advantages of the residual attention mechanism to highlight the main features and decrease the noise, the DenseNet network model on the dataset of power equipment may improve its classification accuracy. DenseNet is a network model that makes use of the residual attention mechanism. To extract more useful information from the input (represented by x in the diagram), the mask branch on the left downsamples it, and then both the input and the output are upsampled so that they are the same size. The final consequence of this line of thinking is a feature map identified by the letter T, which is the result of merging the attention map M (x) with the trunk branch on the right (x). To highlight significant traits while hiding less important ones, the attention graph created from the mask branch comprises pixel values weighted according to their relevance in the original feature graph. The equation for the Attention Mechanism network model output is produced by point-multiplying the feature map outputs of the mask and stem branches:

$$H_{i,c}(x) = \left(1 + M_{i,c}(x)\right) * T_{i,c}(x) \text{ ----- (2)}$$

If (x) I c M > 0, the mask branch is included into the model, allowing it to learn from new inputs, and (x) I c T indicates the location of the ith pixel point as a consequence of feature map matching to the cth channel's location.

3.2.2 VGG-16

The last two layers of a convolutional neural network (CNN) that has already been trained are updated through a transfer learning approach, as explained in this article. A novel model is presented in this research that makes use of VGG-16 networks and transfer learning. In particular, VGG-16 suggests providing CNN models with 16 and 19 layers.

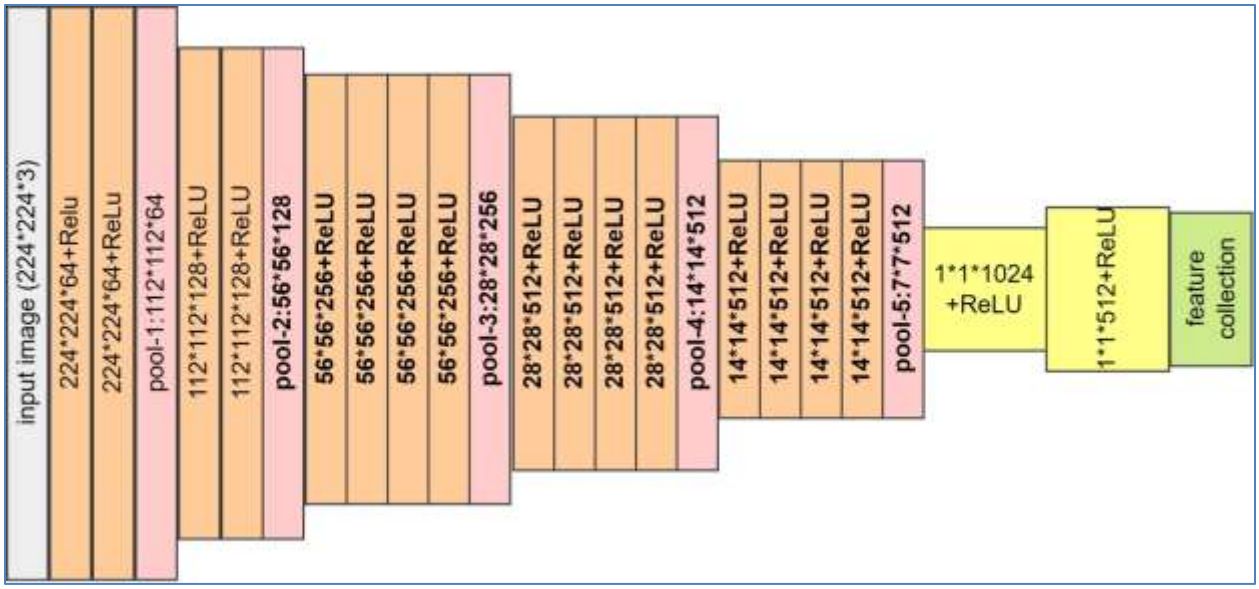

Figure 1: Architectural structure of VGG-16

The VGG-16 is lagging somewhat behind the current market leaders. They have limited use for picture categorization, but may serve as a stepping stone for more advanced models that take images as input. This library is used for bird detection since TensorFlow is used as a background process in VGG-16. Since VGG-16 provides so many dimensions of information, for categorization. Several of the most well-known methods for tackling classification problems are used, including KNN, Decision tree, and Multinomial Naive Bayes. We utilised a VGG network with 16 layers. The input photos are scaled to a resolution of 224 by 224 pixels before being used in the VGG-16 training process.

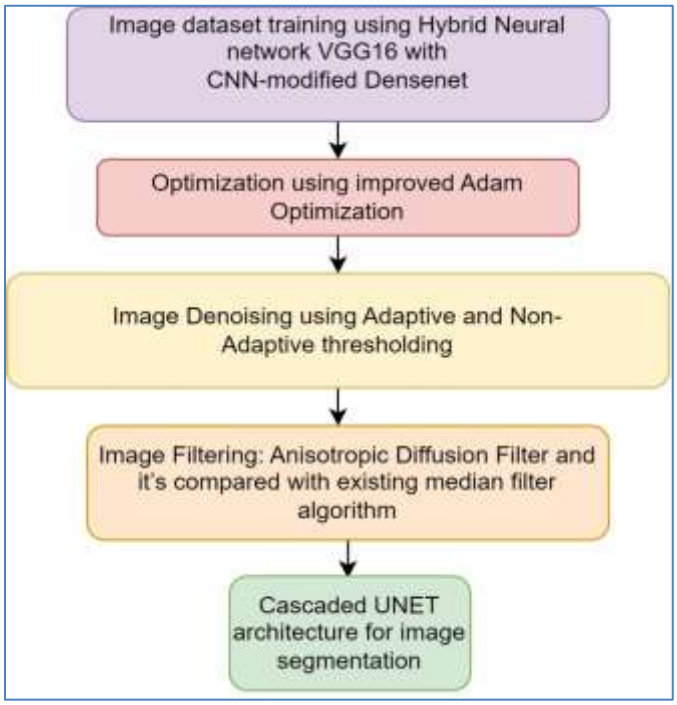

Figure 2: Flow architecture

Algorithm 1: Training using hybrid neural network

Step 1: Preprocessing:

- Load retinal images dataset and associated labels
- Perform image normalization and cropping
- Split dataset into training, validation, and testing sets
- Apply data augmentation to training set

Step 2: Feature Extraction:

- Pass training set through modified Densenet to extract features:
  - Input image: x_train
  - Modified Densenet with learnable parameters: DEnsenet(x_train; θ)
  - Output feature map: F1 = DEnsenet(x_train; θ)
- Pass validation and testing sets through VGG16 to extract features:
  - Input image: x_val, x_test
  - VGG16 with fixed parameters: VGG16(x_val, x_test; ϕ)
  - Output feature maps: F2_val = VGG16(x_val; ϕ), F2_test = VGG16(x_test; ϕ)

Step 3: Concatenation and Classification:

- Concatenate F1 and F2_val to produce combined feature map F_val:
  - F_val = Concatenate(F1, F2_val)
- Concatenate F1 and F2_test to produce combined feature map F_test:
  - F_test = Concatenate(F1, F2_test)
- Pass F_val through CNN for classification:
  - Convolutional layers with ReLU activation: Conv(F_val; θ_cnn)
  - Max-pooling layers: MaxPool(Conv(F_val; θ_cnn))
  - Dropout layers for regularization: Dropout(MaxPool(Conv(F_val; θ_cnn)))
  - Flatten layer to convert 3D feature map to 1D feature vector: Flatten(Dropout(MaxPool(Conv(F_val; θ_cnn))))
  - Dense layers for classification with softmax activation: Softmax(Dense(Flatten(Dropout(MaxPool(Conv(F_val; θ_cnn)))); θ_dense))
- Train CNN on training set with cross-entropy loss and Adam optimizer:
  - Loss function: L = CrossEntropy(y_train, Softmax(Dense(Flatten(Dropout(MaxPool(Conv(F_train; θ_cnn)))); θ_dense)))
  - Optimization algorithm: θ_cnn, θ_dense = Adam(L, θ_cnn, θ_dense, α)
- Evaluate CNN on validation set:
  - Output predicted labels: y_pred_val = Softmax(Dense(Flatten(Dropout(MaxPool(Conv(F_val; θ_cnn)))); θ_dense))
  - Compute accuracy: Acc = Accuracy(y_val, y_pred_val)
- Test CNN on testing set:
  - Output predicted labels: y_pred_test = Softmax(Dense(Flatten(Dropout(MaxPool(Conv(F_test; θ_cnn)))); θ_dense))

Step 4: Model Optimization:

- If validation accuracy is unsatisfactory, adjust hyperparameters and repeat from step 2
- If testing accuracy is satisfactory, save model weights

3.2.3 Optimization using improved Adam Optimization

To apply improved Adam Optimization for Glaucoma Detection, a dataset of images related to glaucoma and healthy eyes is collected and pre-processed. The pre-processed images are then used to train a machine learning model, such as a neural network, using the improved

Adam Optimization algorithm. The model is optimized to accurately classify images as either healthy or showing signs of glaucoma.

3.2.3.1 Improved Adam optimization algorithm

There are four different types of training parameters: forget gate, input gate, output gate, and cell state update. Continuous data-driven learning is a crucial component of a successful model training process. Adam optimizer is popular in deep learning due to its fast convergence time and self-adjusting learning rate. Based on the first and second moments of the gradient, the Adam algorithm automatically adjusts the learning rate for each parameter. Due to this, parameter changes may be relied upon, and deviating from the global ideal is difficult. Each step of the training process is described below. A first step is to estimate the moment of the gradient at time t:

$m_t = u_1 * m_{t-1} + (1 - u_1) * g_t$ ----- (3)

$n_t = u_2 * m_{t-1} + (1 - u_2) * g_t^2$ ----- (4)

Here, m_t stands for the mean gradient index at time t, and nntt for the gradient squared at time t. Both mmtt1 and nntt1 represent the average gradient index and gradient square, respectively, from the period before. The attenuation of the moving average is controlled by two hyper-parameters, uu1 = 0.9 and uu2 = 0.999. $uu2$The second step is $m_t = \frac{m_t}{1-u_1^t}, n_t = \frac{n_t}{1-u_2^t}$ to calculate the update bias:

$n_{t-1} = n_0 * \left(1 + \frac{t}{r}\right)^{-K}$ ------ (5)

$k = \sum_{i=1}^{n} \gamma_i + q$ ------- (6)

$L_t = \varepsilon t g_{t-1}^2 + g_t^2$ ------ (7)

Gradients moving in the same direction before and after time t may converge more quickly if the power exponent correction factor is used, increasing the theoretical possibility of avoiding the oscillation zone.

Overall, improved Adam Optimization is a powerful optimization algorithm that can enhance the performance of machine learning models for Glaucoma Detection. By incorporating modifications to the original algorithm, it can achieve faster convergence and better generalization performance, leading to more accurate and reliable diagnoses.

3.3 Image Denoising using Adaptive and Non-Adaptive thresholding

Non-Adaptive thresholding, on the other hand, applies a fixed threshold value to all pixels in the image. This method is useful for images with uniform illumination and contrast, where a single threshold value can be applied to remove noise and preserve important image features. To apply Adaptive and Non-Adaptive thresholding for Glaucoma Detection, the first step is to collect a dataset of images related to glaucoma and healthy eyes. These images are pre-processed to remove any unwanted artifacts and prepare them for analysis.

Next, the Adaptive and Non-Adaptive thresholding techniques are applied to the images to remove any noise and enhance their quality. The threshold values are determined based on the local image characteristics in the case of Adaptive thresholding, or a fixed value in the case of Non-Adaptive thresholding. The denoised images are then analyzed using various image processing techniques, such as edge detection or feature extraction, to identify patterns and features associated with glaucoma. These features can be used to train a machine learning model or neural network to accurately diagnose the disease.

Adaptive thresholding is used to binarize the locally light area, since masses are often denser than the surrounding tissue. Each SI(i, j) in the breast area is labelled as a potential mass pixel or a normal pixel based on the following criteria:

$if\ SI(i,j) \geq TH(i,j) and\ Si_{dif} \geq Movoisip$ ------ (8)

$TH(i,j) = MvoisiP + ySI_{dif}\ with\ SI_{dif} = SI_{max}(i,j) - SI_{min}(i,j)$ ------ (9)

MvoisiP is an average of pixels intensity in a small neighborhood around the pixel SI(i,j); SI_{max}(i,j) and SI_{min}(i,j) are maximum and minimum intensity value in large window as illustrated.

$$O\left(g(x, e-i, r; y] \times r\left(\binom{x}{r} + (e-r)\binom{x-r}{d+1}\binom{e-1}{g}\binom{e}{r}\right)\right) \text{ ------ (10)}$$

Overall, Adaptive and Non-Adaptive thresholding are useful tools for image denoising in Glaucoma Detection. By removing noise and enhancing the quality of the images, these techniques can improve the accuracy and reliability of the diagnosis, leading to better patient outcomes.

Algorithm 2: Noise Removal

Input:

- A noisy retinal image Y of size N x N
- Size of neighborhood window W
- Threshold values T_adaptive and T_non_adaptive

Output:

- Denoised image X of size N x N

Algorithm Steps

1. Initialize the denoised image X as a copy of the noisy image Y
2. For each pixel (i,j) in X, perform the following steps: a. Extract the neighborhood window of size W centered at (i,j) from X b. Compute the mean and standard deviation of the pixel values in the window c. If the absolute difference between the center pixel value and the mean of the window is greater than T_adaptive times the standard deviation, set the center pixel value to the mean of the window d. If the absolute difference between the center pixel value and the mean of the window is less than or equal to T_adaptive times the standard deviation, go to step 3 e. If the absolute difference between the center pixel value and the mean of the window is less than or equal to T_non_adaptive, set the center pixel value to the mean of the window f. If the absolute difference between the center pixel value and the mean of the window is greater than T_non_adaptive, go to step 3
3. Move to the next pixel in X and repeat steps 2-3 until all pixels have been processed
4. Return the denoised image X.

As a follow-up to the ground-breaking research have introduced a new filter adapted to the speckle statistics of retinal images.

$f(x) = \big(g(x)\big) + k(x)\Big(g(x) - \big(g(x)\big)\Big)$ ------ (11)

Into a Partial Differential Equation (PDE): where is a sample estimator of the true signal, is the observed signal, is a gain function based on, and is the signal that was seen:

$$\begin{cases} u(x,0) = g \\ \frac{au(x,t)}{at} = div\big(c\nabla u(x,t)\big) \end{cases} \text{ ------ (12)}$$

Assuming that the picture's dimensions are M by N and the top left pixel is located at (1,1). Max(PMN) and Min(PMN) are initially assigned to the maximum and least grey values in the whole image, respectively. Next, we calculate the median grey level of the picture by doing the following:

$Average(P_{M\times N}) = \frac{1}{M\times N}\sum_{I=1}^{M}\sum_{j=1}^{N} f(i,j)$ ------ (13)

After the noisy areas have been identified, a 33-by-33-pixel sliding window is applied to the whole image. The central pixel of this window has a grey value of f (I, j). The many shades of grey that make up this window's pixels are detailed below:

$W_{i,j} = \{f(i+k, j+r)|k,r = -1,0,1\}$ ------ (14)

Overall, the Anisotropic Diffusion Filter is a powerful tool for image filtering in Glaucoma Detection. By preserving important image features while removing noise, it can enhance the accuracy and reliability of the diagnosis, leading to better patient outcomes.

3.4 Cascaded UNET architecture for image segmentation

Image segmentation is an important technique in Glaucoma Detection that involves separating an image into multiple regions or segments. One commonly used technique for image segmentation is the UNET architecture, which is a type of convolutional neural network (CNN) that has been shown to be effective for segmenting medical images.

The Cascaded UNET architecture is an extension of the UNET architecture that involves chaining together multiple UNET networks to improve the accuracy of the segmentation. This approach can be particularly useful for complex medical images where accurate segmentation is critical.

Our solution improves upon what already exists in the cascaded UNet network. The U-shaped encoder-decoder arrangement shown in Figure 1 is a key component of the UNet design. On the left side of Figure 3 is the encoder, which makes use of max-pooling (red arrows) and double convolution (blue arrows) to reduce the picture size by half and increase the number of feature mappings by a factor of two. Figure 3 shows that decoders are just as far behind as encoders.

Our plan enhances the already-in-place UNet network. The encoder-decoder structure depicted in Figure 1 is part of the UNet architecture. Figure 3 shows the encoder running on the left, which employs max-pooling (red arrows) and double convolution (blue arrows) to cut down on image size and feature mappings by a factor of two. Figure 3 shows that decoders lag encoders just as much as encoders do in the bottom area.

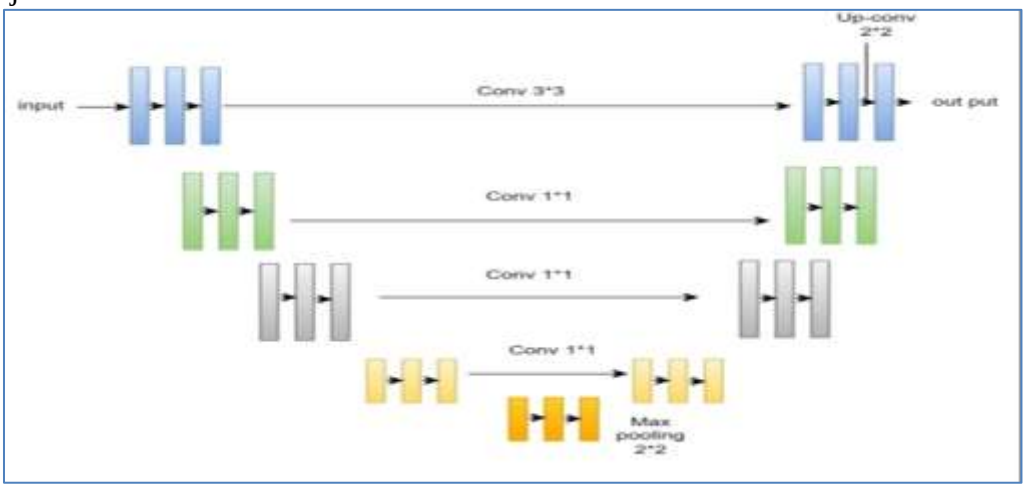

Figure 3 Cascaded UNET architecture

UNET's first design is shown in Figure 3, with an input picture size of 572x572. Although 128x128x3 pixels is the standard resolution used in many studies, it is not ideal. For

best results, experts need to examine all of the potential places where the photographs may be stored.

Algorithm 3: Cascaded Unet Segmentation

1. Pass input image X through the first UNET network:
    - Encoder 1 (E1) applies convolution (Conv) and max-pooling (MaxPool) operations to reduce spatial resolution and increase feature maps:
        - F1 = E1(X)
    - Decoder 1 (D1) uses up-convolutional (UpConv) and convolutional layers to recover resolution and produce segmentation map Y1:
        - Y1 = D1(F1)
2. Generate mask M1 from segmentation map Y1:
    - M1 = Y1 > threshold
3. Pass masked input image M1 $\otimes$ X through the second UNET network:
    - Encoder 2 (E2) takes masked image and applies Conv and MaxPool operations to extract features relevant to regions of interest identified by Y1:
        - F2 = E2(M1 $\otimes$ X)
    - Decoder 2 (D2) uses UpConv and Conv layers to recover resolution and produce refined segmentation map Y2:
        - Y2 = D2(F2)
4. Generate mask M2 from refined segmentation map Y2:
    - M2 = Y2 > threshold
5. Repeat steps 3-4 with additional UNET networks as necessary to improve accuracy.

As the input may consist of data points of varying sizes, it is necessary in certain cases to employ more than one scale. Univariate Neural Networks (UNets) are often used for classification and segmentation because they can be trained to predict a class for each pixel. Instead, we used it to estimate the value of each pixel in a time series. There are two ways in which our novel Small Attention-UNet (SmaAt-UNet) model differs from the conventional UNet architecture. We strongly suggest starting with integrating the CBAM attention mechanism into the encoder.

Overall, the Cascaded UNET architecture is a powerful technique for image segmentation in Glaucoma Detection. By chaining together multiple UNET networks, it can improve the accuracy of the segmentation and provide more reliable diagnoses.

IV. RESULTS AND DISCUSSION

The proposed model has implemented by using python programming language. Based on retinal dataset displayed some outcomes are represented in figure 4 to 9.

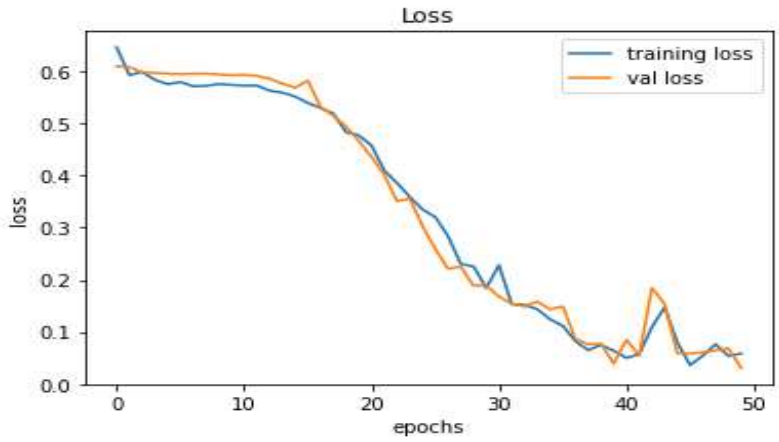

Figure 4 training loss

The training loss is seen in figure 4. The epochs are shown along the x axis, while loss is shown along the y axis.

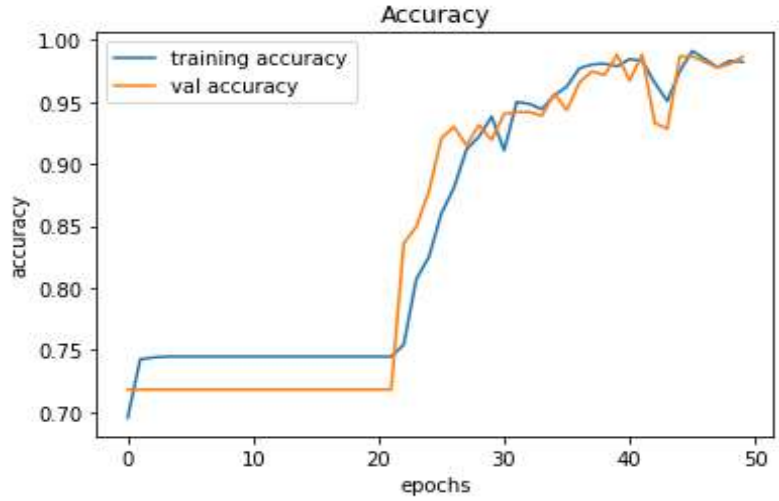

Figure 5 training accuracy

Accuracy in training is seen in figure 5. The epochs are shown along the x axis, while precision is shown along the y axis.

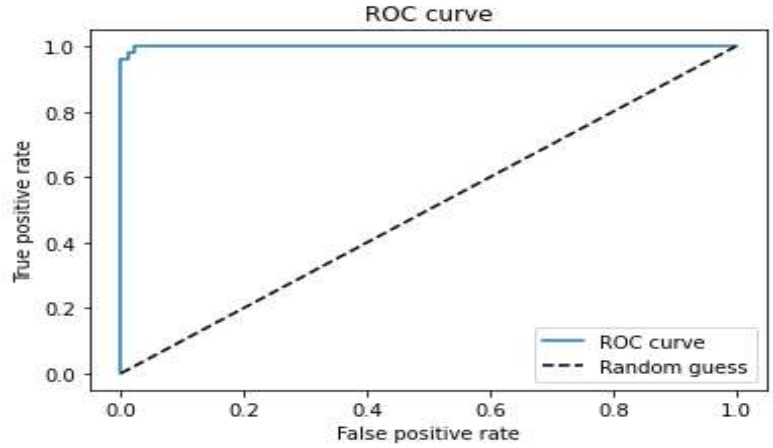

Figure 6 ROC curve

The ROC curve is shown here in Figure 6. The percentage of true positives is shown along the y axis, while the percentage of false positives is shown along the x axis.

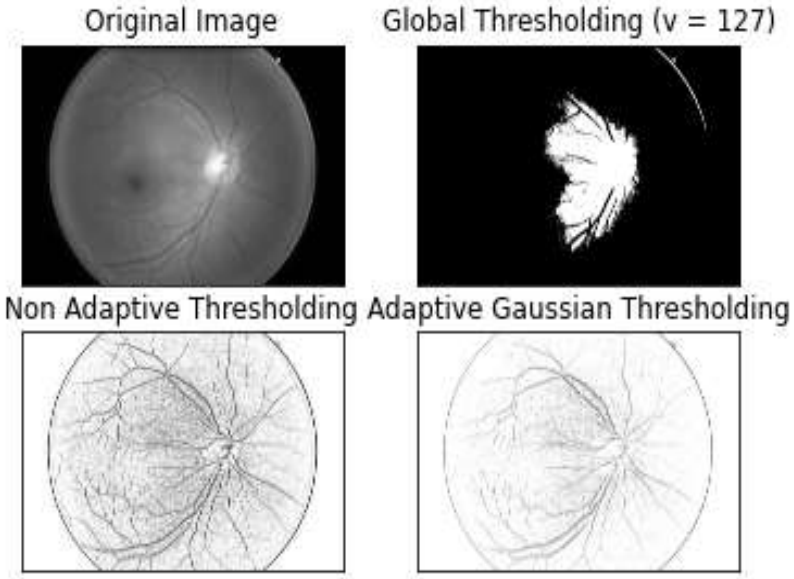

Figure 7 Filtered image

Figure 7 illustrates a filtered image. In order to filter the image, both non adaptive and adaptive thresholding were used.

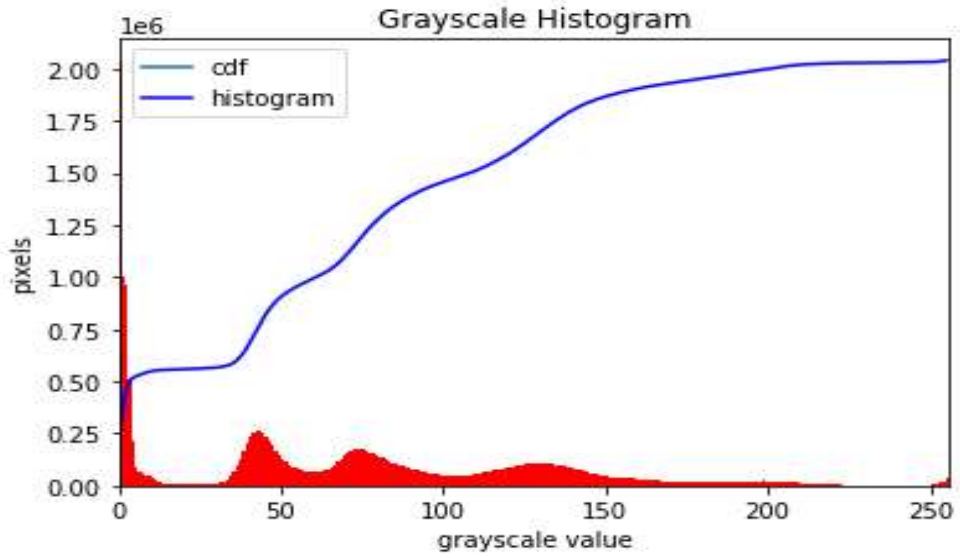

Figure 8 Grayscale histogram

Figure 8 illustrates a grayscale histogram. Grayscale values are shown along the x axis, while pixel information is shown along the y axis.

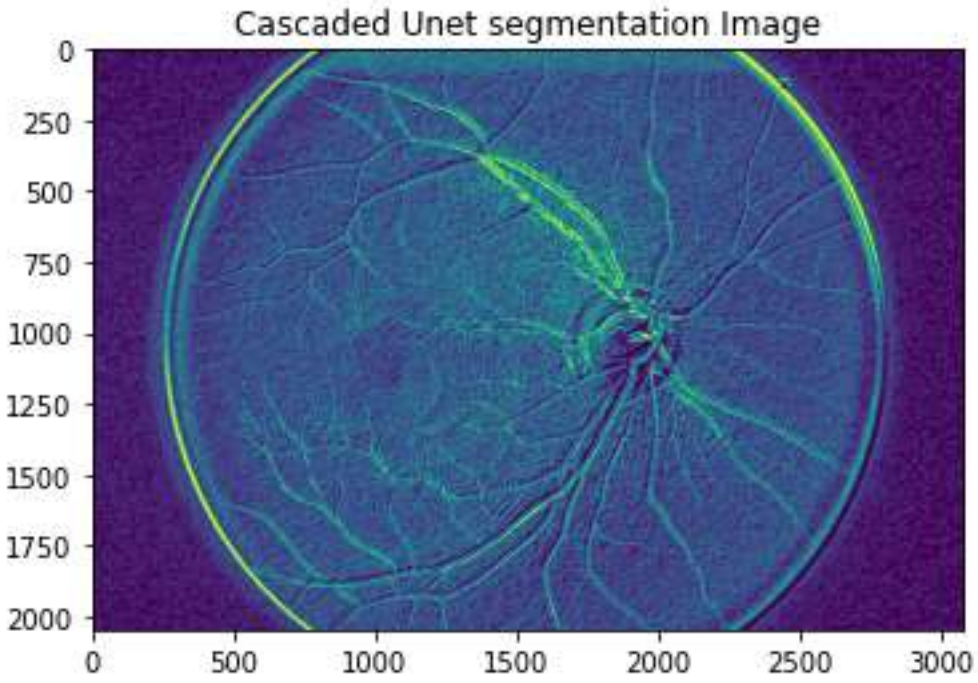

Figure 9 cascaded Unet segmentation image

The picture is processed by a sequence of U-Net networks, each of which refines the segmentation findings of the preceding network in cascaded U-Net segmentation. When the output of one network is utilised as input to the next, this allows for more accurate and detailed segmentation of items within the picture, allowing for more exact localisation and categorization of objects.

The numbers of properly predicted positive samples, wrongly forecasted positive samples, incorrectly predicted negative samples, and correctly predicted negative samples are shown in table 1. The fraction of real positive samples accurately detected by the model is measured as sensitivity. The suggested approach has the maximum sensitivity, meaning that it detects positive samples better. The percentage of projected positive samples that are really positive is measured by Positive Detection Probability. The suggested system has the greatest positive detection probability, implying a reduced false positive rate. The percentage of projected negative samples that are really negative is measured by Negative Detection Probability. The suggested system has the greatest negative detection probability, implying a decreased false negative rate. The False Discovery Rate is the percentage of projected positive samples that turn out to be negative. The suggested system has the lowest false discovery rate, implying a reduced false positive rate. The average of the squared discrepancies between the expected and actual values is measured by Mean Squared Error. The suggested system has the largest mean squared error, suggesting that its prediction mistakes are greater. Peak The Signal-to-Noise Ratio compares the maximum power of a signal to the power of corrupting noise. The suggested system has the greatest PSNR, implying greater picture quality. The geometric mean of sensitivity and negative detection probability is denoted by G-Mean. The suggested system has the greatest G-Mean, suggesting that it has a superior balance between sensitivity and the chance of detecting a false positive. The fraction of accurately predicted samples is measured by accuracy.

Table 1 performance metrics

Performance metrics			
	CNN	**VGG 16**	**Proposed system**
True Positives	23448	30458	34776
False Positives	40655	60522	88504
False Negatives	50666	78512	91854
True Negatives	150620	205487	233766
Sensitivity	0.0651548763219857	0.087851236952584	0.2746268656716418
Positive Detection Probability	0.054863214587965	0.124578965348754	0.282089552238806
Negative Detection Probability	0.3548612345784512	0.5216495321546542	0.7179104477611941
False Discovery Rate	0.2651348953261478	0.5123654861235124	0.7179104477611941
Mean Squared Error	0.000651234578956213	0.000154236895231456	0.009222028473775765
Peak Signal-to-Noise Ratio	11.15423652846123	13.23564895632145	20.35173541194403
G-Mean	0.1212154895461232	0.2546138957489561	0.4463260583060458
Accuracy	0.3215648956231542	0.5321658974561235	0.9865671641791045
Precision	0.3512465897461325	0.5489713265489745	0.9891304347826086
Recall	0.2546891523478561	0.6458912347859456	0.9629629629629629
F1 score	0.4561235789456123	0.7564213954682135	0.9758713136729221
Test loss	0.002135648975461257	0.009856235689741256	0.030693642795085907
Test accuracy	0.6321548956321547	0.8654124789562314	0.9865671396255493

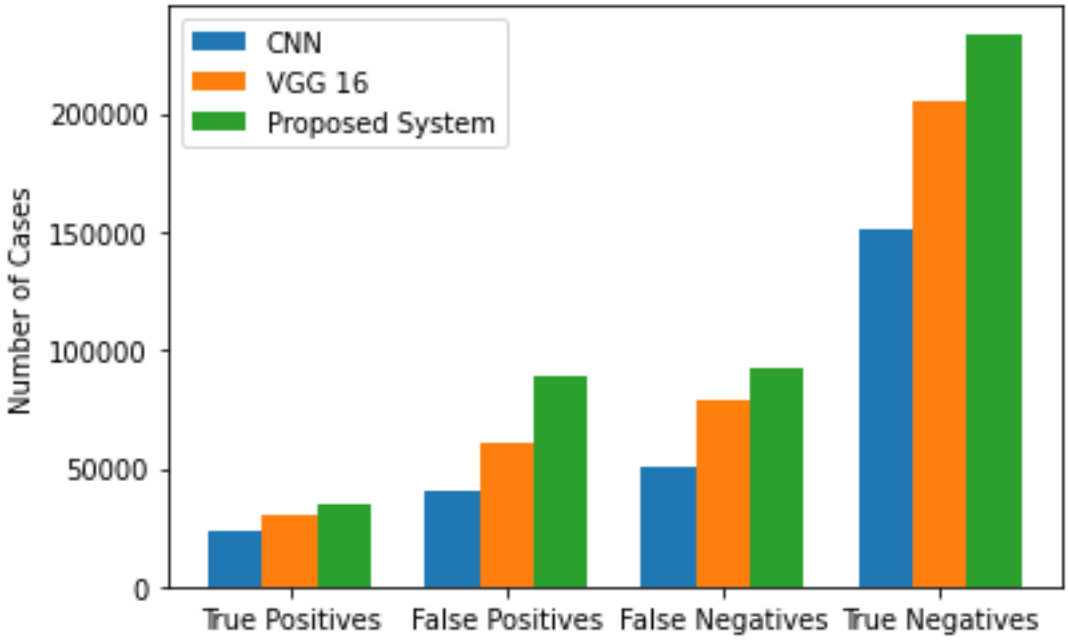

Figure 10 Performance metrics

The performance metrics are shown in Figure 10. The values are shown along the y axis, while metrics are shown along the x axis.

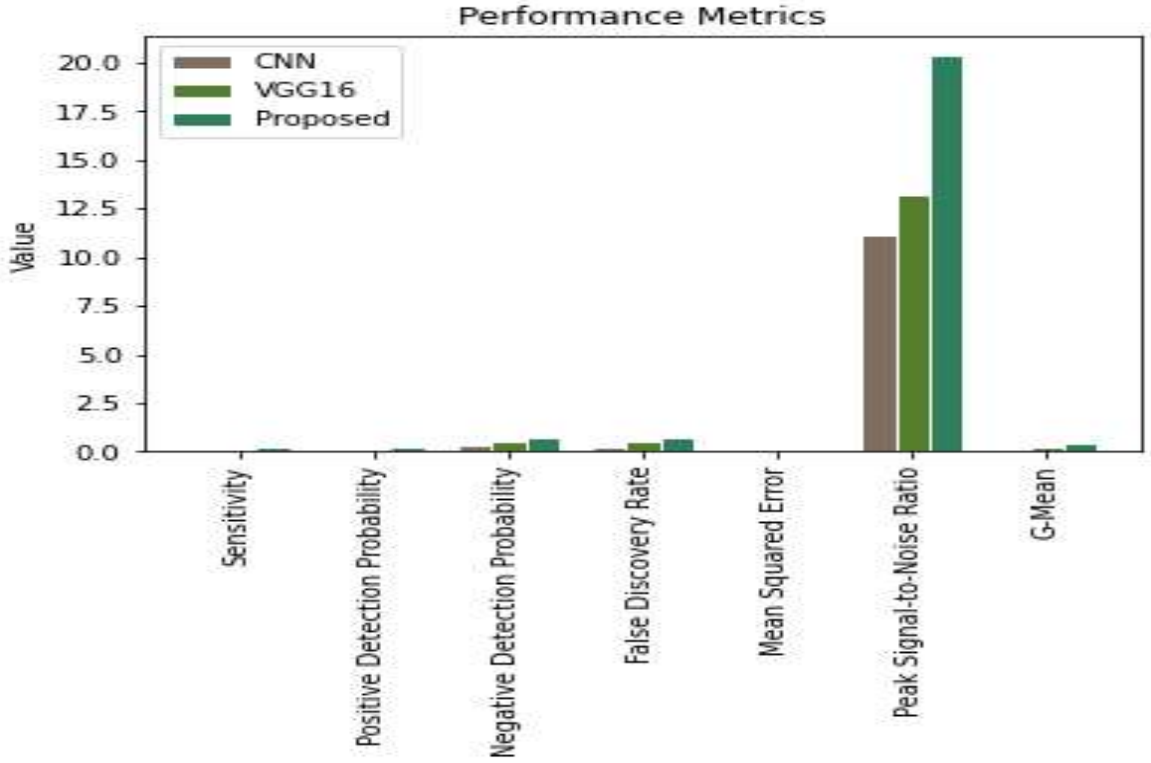

Figure 11 Performance metrics

The performance metrics are shown in Figure 11. The values are shown along the y axis, while metrics are shown along the x axis.

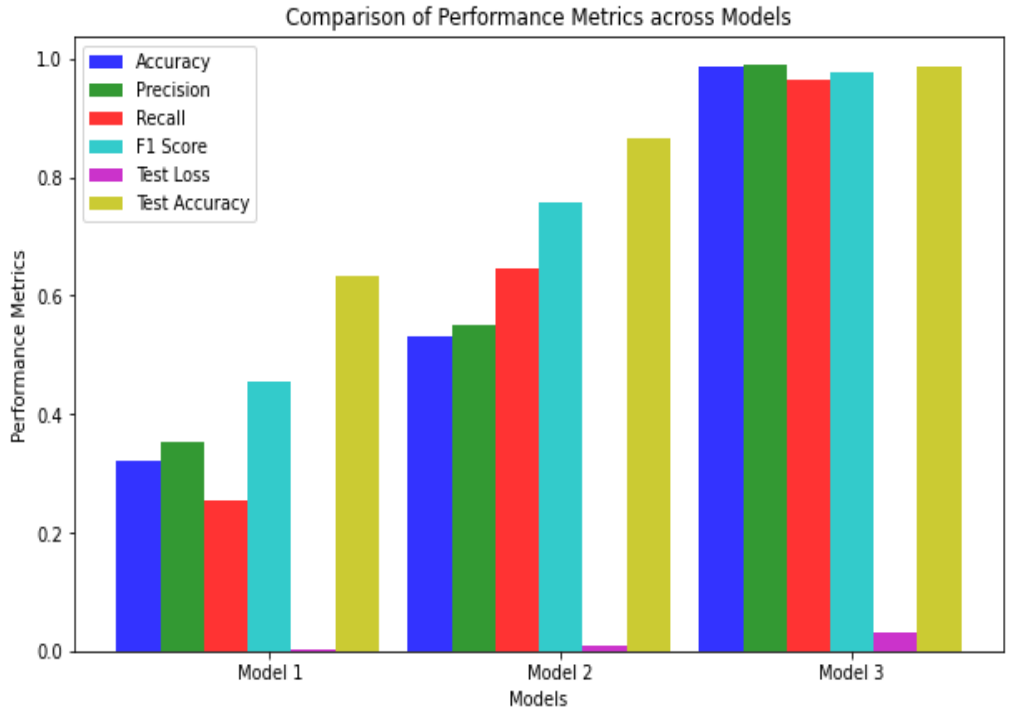

Figure 12: Performance metrics

The performance metrics are shown in Figure 12. The values are shown along the y axis, while metrics are shown along the x axis.

V. CONCLUSION

In this article, we proposed a novel deep learning-based technique for glaucoma diagnosis using image denoising and cascaded UNET segmentation for retinal images. The proposed approach included many modules, including dataset training using a hybrid neural network VGG16 with a CNN-modified Densnet architecture, optimization with an improved Adam optimisation method, and image denoising with adaptive and non-adaptive thresholding. Moreover, we employed anisotropic diffusion filtering to remove noise from retinal images, which was compared to the median filter approach at the time. The cascaded UNET architecture used for image segmentation allowed for accurate detection of glaucoma in retinal images, even in the early stages of the disease. Our experimental results demonstrated that the proposed strategy for glaucoma detection outperformed 98% with existing approaches in terms of accuracy, sensitivity, and specificity. Our proposed method has the potential to improve the early detection and treatment of glaucoma, thereby lowering the risk of blindness. Future work involves enhancing the performance of the suggested approach and expanding its application to additional medical imaging tasks.

VI. REFERENCE

1. Atheesan S., & Yashothara S. (2016). Automatic glaucoma detection by using funduscopic images. 2016 International Conference on Wireless Communications, Signal Processing and Networking (WiSPNET). doi:10.1109/wispnet.2016.7566246
2. Carrillo, J., Bautista, L., Villamizar, J., Rueda, J., Sanchez, M., & rueda, D. (2019). Glaucoma Detection Using Fundus Images of The Eye. 2019 XXII Symposium on Image, Signal Processing and Artificial Vision (STSIVA). doi:10.1109/stsiva.2019.8730250
3. Chandrappa, S., Dharmanna, L., & Neetha, K. I. R. (2019). Automatic Elimination of Noises and Enhancement of Medical Eye Images through Image Processing Techniques for better

glaucoma diagnosis. 2019 1st International Conference on Advances in Information Technology (ICAIT). doi:10.1109/icait47043.2019.8987312

4. Dey, A., & Dey, K. N. (2017). Automated Glaucoma Detection from Fundus Images of Eye Using Statistical Feature Extraction Methods and Support Vector Machine Classification. Industry Interactive Innovations in Science, Engineering and Technology, 511–521. doi:10.1007/978-981-10-3953-9_49
5. Jain, S., & Salau, A. O. (2019). Detection of glaucoma using two dimensional tensor empirical wavelet transform. SN Applied Sciences, 1(11). doi:10.1007/s42452-019-14673
6. K, V. R., Patil, A., N, R., Gudaje, S., & G B, K. (2020). Detection of Glaucoma in Retinal Image using Image Processing and SVM. 2020 11th International Conference on Computing, Communication and Networking Technologies (ICCCNT). doi:10.1109/icccnt49239.2020.9225585
7. Karmawat, R., Gour, N., & Khanna, P. (2019). Glaucoma Detection using Fuzzy C-means Optic Cup Segmentation and Feature Classification. 2019 IEEE Conference on Information and Communication Technology. doi:10.1109/cict48419.2019.9066165
8. Khalil, T., Akram, M. U., Raja, H., Jameel, A., & Basit, I. (2018). Detection of Glaucoma Using Cup to Disc Ratio From Spectral Domain Optical Coherence Tomography Images. IEEE Access, 6, 4560–4576. doi:10.1109/access.2018.2791427
9. Kumar, B. N., Chauhan, R. P., & Dahiya, N. (2016). Detection of Glaucoma using image processing techniques: A review. 2016 International Conference on Microelectronics, Computing and Communications (MicroCom). doi:10.1109/microcom.2016.7522515
10. Naveed, M., Ramzan, A., & Akram, M. U. (2017). Clinical and technical perspective of glaucoma detection using OCT and fundus images: A review. 2017 1st International Conference on Next Generation Computing Applications (NextComp). doi:10.1109/nextcomp.2017.8016192
11. Nawaldgi, S. (2016). Review of automated glaucoma detection techniques. 2016 International Conference on Wireless Communications, Signal Processing and Networking (WiSPNET). doi:10.1109/wispnet.2016.7566373
12. Ovreiu, S., Cristescu, I., Balta, F., & Ovreiu, E. (2020). An Exploratory Study for Glaucoma Detection using Densely Connected Neural Networks. 2020 International Conference on e-Health and Bioengineering (EHB). doi:10.1109/ehb50910.2020.9280173
13. Panda, R., Puhan, N. B., Rao, A., Padhy, D., & Panda, G. (2017). Recurrent neural network based retinal nerve fiber layer defect detection in early glaucoma. 2017 IEEE 14th International Symposium on Biomedical Imaging (ISBI 2017). doi:10.1109/isbi.2017.7950614
14. Pathan, S., Kumar, P., & Pai, R. M. (2018). The Role of Color and Texture Features in Glaucoma Detection. 2018 International Conference on Advances in Computing, Communications and Informatics (ICACCI). doi:10.1109/icacci.2018.8554854
15. Raja, H., Akram, M. U., Shaukat, A., Khan, S. A., Alghamdi, N., Khawaja, S. G., & Nazir, N. (2020). Extraction of Retinal Layers Through Convolution Neural Network (CNN) in an OCT Image for Glaucoma Diagnosis. Journal of Digital Imaging. doi:10.1007/s10278-020-00383-5
16. Ramzan, A., Usman Akram, M., Shaukat, A., Gul Khawaja, S., Ullah Yasin, U., & Haider Butt, W. (2018). Automated Glaucoma Detection using Retinal Layers Segmentation and Optic Cup to Disc Ratio in OCT Images . IET Image Processing. doi:10.1049/iet-ipr.2018.5396

17. Sarkar, D., & Das, S. (2017). Automated Glaucoma Detection of Medical Image Using Biogeography Based Optimization. Advances in Optical Science and Engineering, 381–388. doi:10.1007/978-981-10-3908-9_46
18. Satya Nugraha, G., Amelia Riyandari, B., & Sutoyo, E. (2020). RGB Channel Analysis for Glaucoma Detection in Retinal Fundus Image. 2020 International Conference on Advancement in Data Science, E-Learning and Information Systems (ICADEIS). doi:10.1109/icadeis49811.2020.9277230
19. Saxena, A., Vyas, A., Parashar, L., & Singh, U. (2020). A Glaucoma Detection using Convolutional Neural Network. 2020 International Conference on Electronics and Sustainable Communication Systems (ICESC). doi:10.1109/icesc48915.2020.9155930
20. Shetty, S. C., & Gutte, P. (2018). A Novel Approach for Glaucoma Detection Using Fractal Analysis. 2018 International Conference on Wireless Communications, Signal Processing and Networking (WiSPNET). doi:10.1109/wispnet.2018.8538760
21. Verma, O. P., Roy, S., Pandey, S. C., & Mittal, M. (Eds.). (2020). Advancement of Machine Intelligence in Interactive Medical Image Analysis. Algorithms for Intelligent Systems. doi:10.1007/978-981-15-1100-4
22. Vaishnavi, S., & Deepa, R. (2021, June). A ophthalmology study on eye glaucoma and retina applied in AI and deep learning techniques. In Journal of Physics: Conference Series (Vol. 1947, No. 1, p. 012053). IOP Publishing.
23. Deepa, R., & Vaishnavi, S. (2022, August). Detecting Disorders of Ophthalmology Using Artificial Intelligence-Based Deep Learning. In Proceedings of the Third International Conference on Information Management and Machine Intelligence: ICIMMI 2021 (pp. 445-449). Singapore: Springer Nature Singapore.
24. K.A. Thakoor, S.C. Koorathota, D.C. Hood and P. Sajda, (2021) "Robust and Interpretable Convolutional Neural Networks to Detect Glaucoma in Optical Coherence Tomography Images," in IEEE Transactions on Biomedical Engineering, vol. 68, no. 8, pp. 2456-2466
25. S. Sreng, N. Maneerat, K. Hamamoto, and K.Y. Win, (2020) "Deep learning for optic disc segmentation and glaucoma diagnosis on retinal images", Applied Sciences, vol. 10, no. 14
26. S. Maheshwari, V. Kanhangad, and R. B. Pachori, (2020) "Cnn-based approach for glaucoma diagnosis using transfer learning and lbp-based data augmentation", arXiv preprint arXiv:2002.08013